

Analysis of the spiral structure in a simulated galaxy

M. Dolores Mata-Chávez,¹★ Gilberto C. Gómez¹ and Ivânio Puerari²

¹*Centro de Radioastronomía y Astrofísica, Universidad Nacional Autónoma de México, Apdo. Postal 3-72, Morelia Mich. 58089, Mexico*

²*Instituto Nacional de Astrofísica, Óptica y Electrónica, Apdo. Postal 51 y 216, 72840 Santa María Tonantzintla, Puebla, Mexico*

Accepted 2014 August 14. Received 2014 August 13; in original form 2014 January 22

ABSTRACT

We analyse the spiral structure that results in a numerical simulation of a galactic disc with stellar and gaseous components evolving in a potential that includes an axisymmetric halo and bulge. We perform a second simulation without the gas component to observe how it affects the spiral structure in the disc. To quantify this, we use a Fourier analysis and obtain values for the pitch angle and the velocity of the self-excited spiral pattern of the disc. The results show a tighter spiral in the simulation with gaseous component. The spiral structure is consistent with a superposition of waves, each with a constant pattern velocity in given radial ranges.

Key words: galaxies: ISM – galaxies: spiral – galaxies: structure.

1 INTRODUCTION

The spiral structure of disc galaxies has been studied for many years now, yet the origin of this structure remains uncertain. Several different theories have been proposed to explain how this structure was formed. The density wave theory (Lin & Shu 1964; Bertin & Lin 1996) proposes quasi-stationary density waves propagating through a rotating disc at constant pattern angular velocity. As an alternative, the swing amplification theory (Goldreich & Lynden-Bell 1965; Julian & Toomre 1966) proposes that the arms arise from smaller perturbations (or perturbations) which add and amplify. This could produce overdensities rotating with the disc. In this model, waves are not quasi-stationary and, therefore when the perturbations cease, the spiral disappears. D’Onghia, Vogelsberger & Hernquist (2013) showed that overdensities could produce non-linear effects in swing amplifications that modify the formation and longevity of the spiral pattern, even after the perturbations have been removed.

In order to study these scenarios, researchers have used N -body simulations. These have been able to reproduce a spiral-like structure generated in many different ways, such as interaction with other galaxies or gravitational instabilities in the disc. Most of these simulations involve a stellar disc only (Quillen et al. 2011; Grand, Kawata & Cropper 2012a,b; Roca-Fàbrega et al. 2013), yet the spiral structure is conspicuous in the gaseous component also (Acreman et al. 2010). Vallée (2005, and references therein) showed that the Galactic stellar spiral structure differs from the gaseous one (see also Gómez, Pichardo & Martos 2013).

Recently, Wada, Baba & Saitoh (2011) and Baba, Saitoh & Wada (2013) showed simulations with stellar and gaseous discs. In those studies, a spiral structure that seems to corotate with the galactic disc is formed.

Several methods have been developed to quantitatively describe the spiral structure in a galactic disc, either in observed images or in a numerical simulations. Using Fourier transformations of images of spiral galaxies, it is possible to obtain estimations of the pitch angle, relative strengths of modes and other parameters of the spiral structure (Davis et al. 2012).

But the issue of the gas role in the formation of the spiral pattern remains unsatisfactorily open. It is usually considered (Bertin & Lin 1996; Dobbs & Baba 2014; Sellwood & Carlberg 2014, for example) that the principal role of the gas is to dynamically cool the stellar disc. Nevertheless, the large-scale interaction of these components has not been properly explored since it is assumed that the small mass of the gaseous disc will have a negligible impact on the dynamics of the stellar one, and so the gaseous component is frequently considered as a perturbation, brushing aside the possible dynamical feedback on the large-scale dynamics. In this paper, we compare the spiral structure of galactic disc with and without a gaseous component using 3D numerical simulations. We use Fourier transforms to measure the parameters of the spiral pattern of the discs. In Section 2, we describe the simulations performed. In Section 3, we present the analysis of the spiral structure in the simulations performed. Finally, we present a summary in Section 4.

2 METHOD

Our simulation contains a galactic disc with $9.8 \times 10^8 M_{\odot}$ of gas and $3.49 \times 10^{10} M_{\odot}$ of stars. Both components are distributed initially with a constant mid-plane density of 0.62 and $0.017 M_{\odot} \text{ pc}^{-3}$ for stars and gas, respectively, out to a radius of 3 kpc. Outside this radius, the mid-plane density follows an exponential profile $\rho = \rho_0 \exp[-(R - R_0)/R_h]$, with $R_0 = 8 \text{ kpc}$, $\rho_0 = 0.15 M_{\odot} \text{ pc}^{-3}$ and $R_h = 3.5 \text{ kpc}$ for the stellar disc, and $\rho_0 = 10^{-2} M_{\odot} \text{ pc}^{-3}$ and $R_h = 8 \text{ kpc}$ for the gaseous disc. In the vertical direction, both components initially follow a Gaussian profile, with scaleheights 0.325 and 0.135 kpc for stars and gas, respectively.

★ E-mail: m.mata@crya.unam.mx

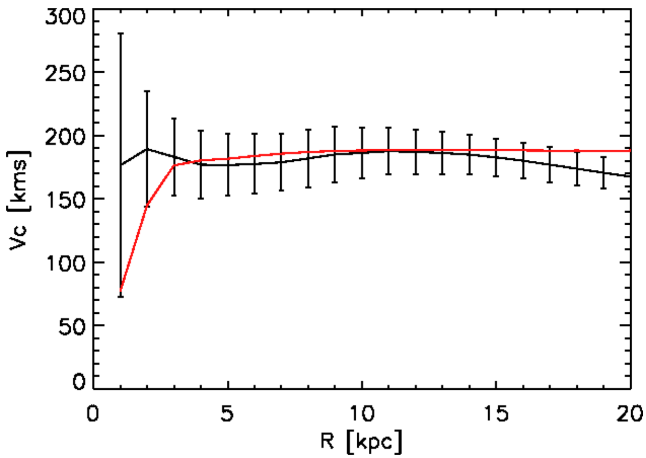


Figure 1. Mean rotational velocity of the simulation. The grey line (red line in online version) corresponds to $t = 0$ Myr and black line to $t = 200$ Myr. The error bars show the standard deviation at different radii.

The particles in the galactic disc are set up in rotational equilibrium with a potential similar to that described in Allen & Santillan (1991), which consist of a halo, a bulge and a stellar disc (see Fig. 1). In addition to the circular velocity, a velocity dispersion of 20 km s^{-1} is added to the stars, and of 12 km s^{-1} to the gas. The Toomre Q parameter for the disc is < 1 in the range $2 < R < 7$ kpc.

The simulation is performed with the *GADGET2* code (Springel, Yoshida & White 2001), which solves the hydrodynamic equations using a smoothed particle hydrodynamics (SPH) algorithm coupled to stellar dynamics. We used 6×10^6 stellar particles and 6×10^6 gas particles, randomly distributed over the disc following the density profile described above. The simulations are set up within a 40 kpc box. The version of the *GADGET2* code we use has a sink particle formation prescription (Jappsen et al. 2005) with a critical density for sink formation of $3 \times 10^3 \text{ cm}^{-3}$.

Since the mass resolution is similar to the masses of giant molecular complexes, it is necessary to consider the gas segregation into phases. To achieve this, the simulation includes the cooling function described in Koyama & Inutsuka (2000).¹ To avoid a prohibitively short time step, we apply the fast cooling model described in Vázquez-Semadeni et al. (2007), which evolves the gas temperature as exponentially approaching the equilibrium temperature at the current density. The segregation of the gas in phases, the dynamics of the dense clouds formed and associated star formation, as modelled by sink particle formation, will be explored in a future work.

We performed two simulations. Simulation I consisted of both stellar and gaseous disc components, while simulation II consisted only of the stellar component, with the same random density and velocity distribution as the stellar disc in simulation I. Simulation I was evolved through 410 Myr, while we were able to evolve simulation II through 923 Myr. In both simulations, the particles start in an unrelaxed state, and so the self-stimulated spiral appears sooner than in relaxed simulations. Nevertheless, since the evolution lasts $3.5\tau_{\text{rot}}$ (where τ_{rot} is the rotation period at the stellar disc scale-length, $\tau_{\text{rot}} = 120 \text{ Myr}$), the evolution should be enough to erase signatures of the initial conditions.

¹ Please note a typographical error in the expression for the cooling function in Koyama & Inutsuka (2000). See Vázquez-Semadeni et al. (2007).

Fig. 2 shows mass surface density maps of the simulations at $t = 200$ Myr for the gaseous disc in simulation I (top) and stars (middle), and the stellar disc in simulation II (bottom). The galaxies in the simulations are not perturbed, so the spiral structure forms due

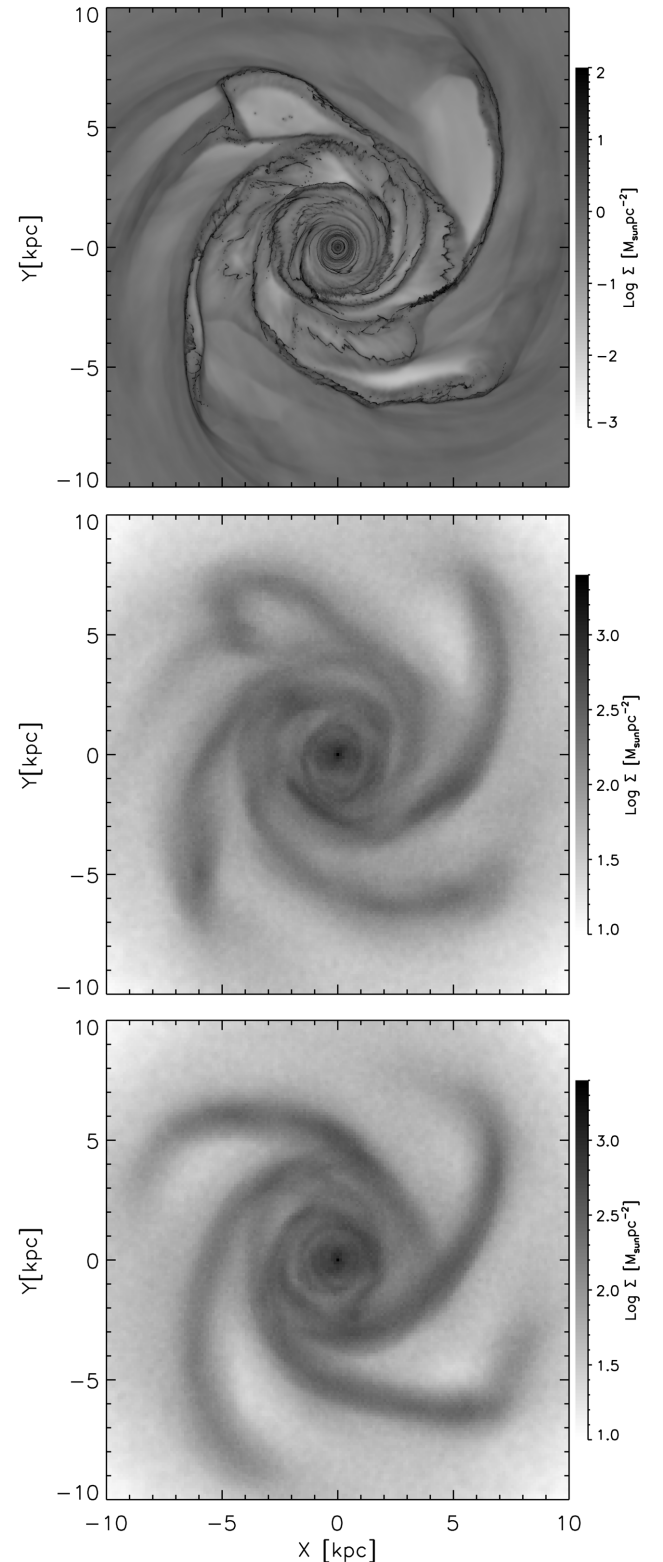


Figure 2. Gaseous (top) and stellar (middle) surface density distributions for simulation I, and stellar surface density (bottom) for simulation II at $t = 200$ Myr. For clarity, only the $r < 10$ kpc is shown.

to self-gravity out of the random fluctuations in the initial particle distribution. In simulation I, the gaseous and stellar disc have similar large-scale structure, namely four spiral arms with basically the same locus, but the stellar arms are thicker than the gaseous ones, with the latter showing much more substructure, as expected. But it is noticeable that the stellar arms in simulation I show more substructure than those in simulation II, the most noteworthy being a ‘hook’ around $(x, y) = (-4, 7)$ kpc, although the overall strength of the arms differs in both simulations. The presence of a gaseous component is known to destabilize a disc (Jog 1996), since the gas is dissipative and is allowed to cool. But, we find that the stellar density in the arms is larger in simulation II, with the spiral arms remaining coherent longer (see Section 3).

3 SPIRAL STRUCTURE

Following Grand et al. (2012b), we describe the spiral structure in the simulations using a Fourier analysis of the mass surface density distributions of stars and gas. Consider the Fourier transform (along the azimuthal angle ϕ , at a given radius r) of the surface density distributions resulting from the simulations, $A(m, r)$, where m is the Fourier mode in question. Since both simulations develop four arms (see Fig. 2), we show the time evolution of the $A(4, r)$ mode in Fig. 3. It can be seen that the four-arm structure is formed between 2 and 5 kpc at $t \sim 30$ Myr, extending to larger radii at later times. But, after ~ 300 Myr, while still the largest, the $m = 4$ mode is no longer dominant since other modes grow in the inner part of the galaxy. After $t \sim 150$ Myr, $A(4, r)$ is significant only in the $5 < R < 10$ kpc range, with its amplitude declining in time.

It is noticeable that the gas component in simulation I has the largest amplitudes, meaning that the gas is more tightly associated with a four-fold symmetric pattern than the stars. Comparing the stellar density in both simulations I and II, we may note that simulation II has larger $A(m, r)$ amplitudes, meaning that in the absence of gas, the spiral structure is enhanced. One possible reason for this is that interactions between stars and giant molecular clouds heat the stellar disc, thus causing the spiral structure intensity to decrease. Since we failed to find a correlation between the stellar velocity dispersion and the gaseous disc surface density (for constant radius rings), we do not think that this is the reason for a weaker spiral when gas is included. Another possible reason is that the spiral structure in simulation I is formed almost at the same time in the stellar and gaseous disc, but with a small phase difference (Shu, Milione & Roberts 1973; Pérez-Villegas, Gómez & Pichardo, in preparation). Even if the gaseous arm is small compared to the stellar arm mass, this out-of-phase perturbation might cause a decrease on the stellar response.

In order to measure the pitch angle for each of the spiral modes that describe the density distribution, consider the amplitudes for the unwound modes,

$$\hat{A}(m, p) = \frac{1}{D} \int_{-\pi}^{+\pi} \int_{u_{\min}}^{u_{\max}} \Sigma(u, \phi) \exp[-i(m\phi + pu)] d\phi du, \quad (1)$$

where $u = \log r$, m is the Fourier mode in question, $p = -m/\tan(\alpha)$ is a logarithmic wavenumber, α is the pitch angle of the spiral, Σ is the mass surface density distribution and D is a normalization given by

$$D = \int_{-\pi}^{+\pi} \int_{r_{\min}}^{r_{\max}} \Sigma(u, \phi) du d\phi. \quad (2)$$

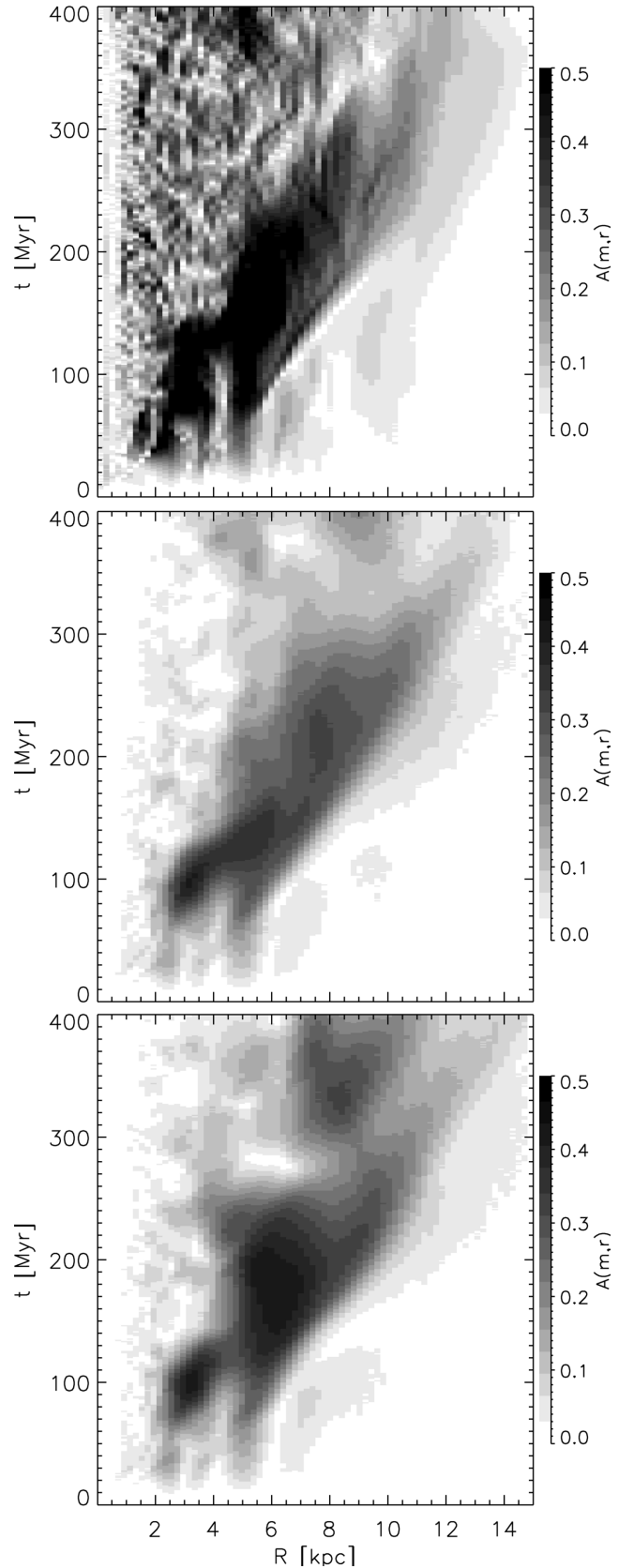


Figure 3. Evolution of the $m = 4$ mode for gas (top) and stars (middle) in simulation I, and stars (bottom) in simulation II.

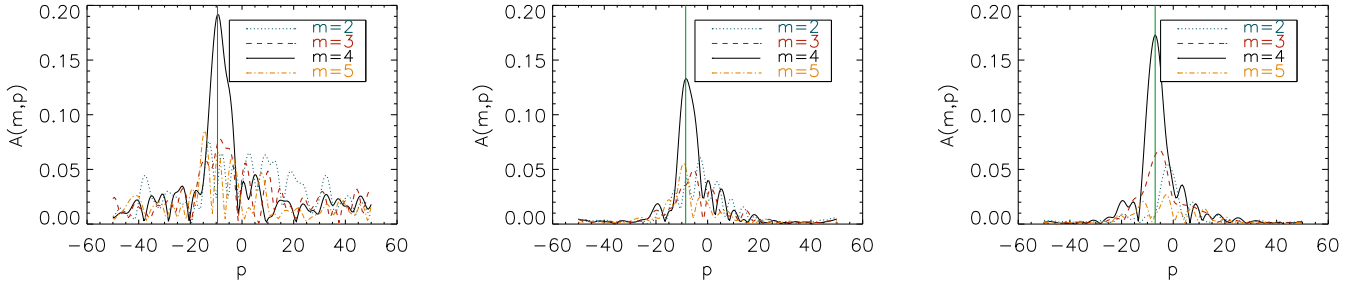


Figure 4. $\hat{A}(m, p)$ for gaseous disc for $t = 200$ Myr (left), for stellar disc $t = 200$ Myr (centre) and stellar disc without gas (right). Lines represent different Fourier modes. The peak of the dominant $m = 4$ mode changes from p -values corresponding to pitch angles of $\alpha = 22^\circ.8$ (left), $25^\circ.2$ (centre) and $29^\circ.7$ (right).

Fig. 4 shows the amplitude $\hat{A}(m, p)$ for several m -values for both simulations. The $m = 4$ mode dominates the distribution for most of the evolution, and so, hence forth, we focus our analysis on this mode.

Fig. 5 shows the evolution of $\hat{A}(4, p)$ during the simulation. In the plot, it can be seen that, even if p remains almost constant, the amplitude $\hat{A}(m, p)$ changes in time. This might be explained if the spiral is formed by a superposition of transient waves that reinforce the pattern, as stated by Sellwood & Carlberg (2014), or as a result of interference of longer lived spiral waves, as proposed by Comarota & Quillen (2012). For simulation I at 200 Myr, the stellar spiral is more open ($\alpha = 25^\circ.2$) than the gaseous one ($\alpha = 22^\circ.8$), in a similar fashion to simulations of gas in a fixed potential (Gómez et al. 2013). For simulation II, the pitch angle at $t = 200$ Myr is $29^\circ.7$, i.e. the simulation without a gaseous disc yields a more open spiral than the simulation with stars only. These values are consistent with an Sc galaxy (Ma 2002).

In order to determine the velocity of the spiral pattern, consider the amplitudes of the Fourier modes transformed again in time, as a function of radius, thus changing from (m, r, t) space to (m, r, Ω_p) . Consider the phase $\Phi = \arctan(A_{\text{Im}}/A_{\text{Re}})$ where A_{Im} and A_{Re} are the imaginary and the real parts of the amplitude. The pattern angular velocity is then given by $\Omega_p = \dot{\Phi}/N$, where $\dot{\Phi}$ is the Fourier transform in time of Φ and N is the total number of data outputs.

Fig. 6 shows the so calculated spectrogram for the $m = 4$ component, along with the orbital frequency Ω of the (initial) axisymmetric disc. It is worth noting that, since the frequency resolution (the Nyquist frequency) is given by the time of the last data output, it is necessary to allow for the longest possible evolution of

the simulation. In our case, simulation I stopped due to numerical issues, but simulation II ran up to 923 Myr. So, the figure shows the spectrogram corresponding to the simulation with the stellar disc only, with 1 Myr between data outputs. As seen from the radial dependence of the amplitude maxima, the frequency for the spiral pattern is not constant but it is composed of a superposition of patterns with different frequencies constant on *restricted* radial ranges, in a manner consistent with the behaviour reported by Sellwood & Carlberg (2014). This superposition of waves is also suggested in the time evolution shown in Fig. 5. If simulation I is used to measure the pattern speed, either with the stellar or gaseous discs, the lower frequency resolution smears these constant Ω_p regions, giving the impression that the spiral arms rotate solidly, similarly to those reported recently (Wada & Koda 2004; Wada et al. 2011; Grand et al. 2012a; Roca-Fàbrega et al. 2013).

4 SUMMARY

In this paper, we performed SPH simulations of galactic discs using an SPH N-BODY code to model a disc with gaseous and stellar components (simulation I) and a disc with stellar component only (II). The gaseous disc is modelled with an explicit cooling function, thus allowing it to segregate into dense and diffuse phases. We observed similar four-arm structure in both simulations but, when a Fourier analysis is performed on the surface density distribution, the spiral structure in simulation II shows a higher $m = 4$ mode amplitude, with less substructure than simulation I, i.e. adding a gaseous component to the simulation leads to more substructure in both stellar and gaseous arms, but it also leads to a weaker stellar

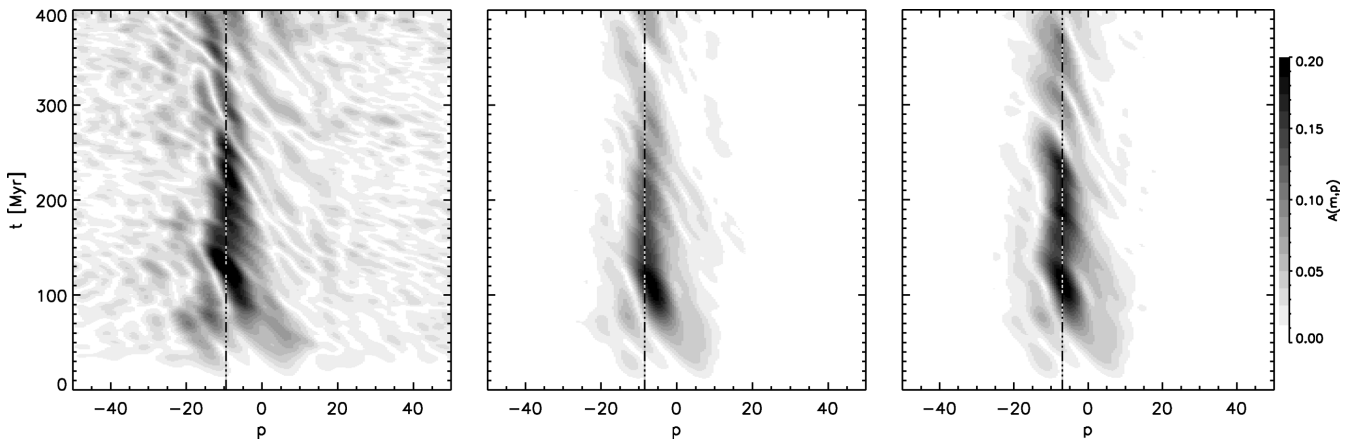


Figure 5. Time evolution of the logarithmic wavenumber, p . The maximum at each time indicates the pitch angle for the gaseous (left) and stellar discs (centre) in simulation I, and the stellar disc in simulation II (right).

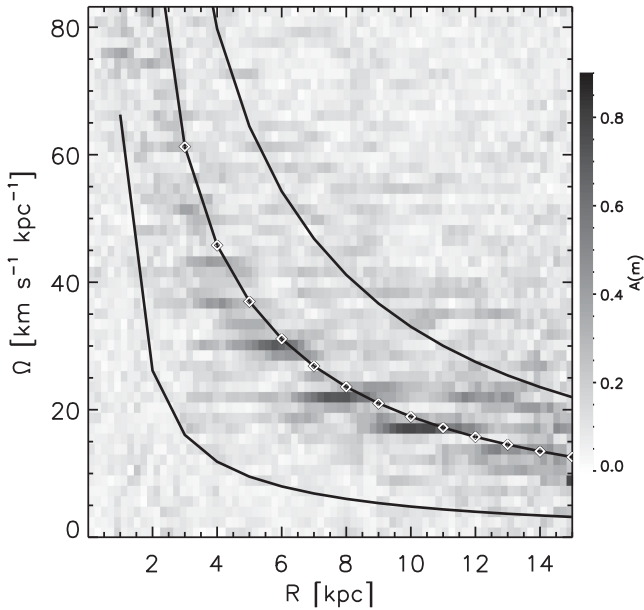


Figure 6. Spectrogram for the $m = 4$ mode in the stellar disc of simulation II for the length of the simulation, i.e. 923 Myr. The line with diamonds corresponds to the angular frequency for the axisymmetric disc, while the upper and lower lines represent the $\Omega \pm \kappa/4$ frequencies.

spiral. We speculate that this might be due to a phase shift between the gaseous and stellar arms, which reduces the coherence of the response to the non-axisymmetric part of the potential. This phase shift between stellar and gaseous spiral arms has been reported before in simulations with fixed spiral potentials (e.g. Shu et al. 1973; Gómez et al. 2013).

The simulations obtained were analysed with a Fourier method to measure the pitch angle and the velocity of the spiral pattern. The spectrogram for simulation II shows that the pattern is better described as a superposition of waves, each with a constant pattern speed in a given radial range. Lack of frequency resolution smears the spectrogram and might make it appear as if the spiral pattern corotates with the disc, as the set of waves, as a whole, follows the rotation of the disc.

About the growth of spiral pattern, Fig. 3 shows the evolution of the spiral structure in our simulations. It can be seen that, even if the spiral structure consists of small fluctuations, it grows globally in a coherent way. D’Onghia et al. (2013) shows that disconnected perturbations serve as seed for the growth of a global spiral pattern through swing amplification, which is favoured by the particles’ self-gravity. In a similar way, overdensities in our simulations generate spiral segments that connect and form a large-scale spiral pattern. The spiral consists of individual segments that rotate with distinct frequencies (as seen in Fig. 6), but still a single global pattern emerges.

With respect to the pitch angles of the pattern, we measure $\alpha = 22.8$ for the gaseous disc, $\alpha = 25.2$ for the stellar disc in simulation I and $\alpha = 29.7$ for the stellar disc in simulation II. A gaseous spiral tighter than the stellar one has been reported in simulations before. But, the fact that the stellar spiral develops a larger

pitch angle when the gas is absent appears counterintuitive considering that the pitch angle is usually more open for disc galaxies of later Hubble type, which have a larger gas content. Further experiments with a range of structural parameters (namely bulge/disc mass ratio or disc/halo scalelength ratio, for example) are necessary to explore the different ways the stellar and gaseous discs generate spiral structure in isolated galaxies.

ACKNOWLEDGEMENTS

The authors wish to thank V. Debattista, E. D’Onghia, A. Pérez-Villegas and J. Sellwood for useful discussions on the subject at hand and an anonymous referee for comments that greatly improved this manuscript. IP thanks the Mexican Foundation CONACyT for financial support. The numerical simulations were performed in the cluster at CRYA-UNAM acquired with CONACyT grants 36571-E and 47366-F to E. Vázquez-Semadeni. This work has received financial support from UNAM-DGAPA PAPIIT grant IN111313 to GCG.

REFERENCES

- Acreman D. M., Douglas K. A., Dobbs C. L., Brunt C. M., 2010, *MNRAS*, 406, 1460
- Allen C., Santillan A., 1991, *Rev. Mex. Astron. Astrofis.*, 22, 255
- Baba J., Saitoh T. R., Wada K., 2013, *ApJ*, 763, 46
- Bertin G., Lin C. C., 1996, *Spiral Structure in Galaxies a Density Wave Theory*. MIT Press, Cambridge, MA
- Comparetta J., Quillen A. C., 2012, preprint ([arXiv:1207.5753](https://arxiv.org/abs/1207.5753))
- Davis B. L., Berrier J. C., Shields D. W., Kennefick J., Kennefick D., Seigar M. S., Lacy C. H. S., Puerari I., 2012, *ApJS*, 199, 33
- Dobbs C., Baba J., 2014, preprint ([arXiv:1407.5062](https://arxiv.org/abs/1407.5062))
- D’Onghia E., Vogelsberger M., Hernquist L., 2013, *ApJ*, 766, 34
- Goldreich P., Lynden-Bell D., 1965, *MNRAS*, 130, 125
- Gómez G. C., Pichardo B., Martos M. A., 2013, *MNRAS*, 430, 3010
- Grand R. J. J., Kawata D., Cropper M., 2012a, *MNRAS*, 421, 1529
- Grand R. J. J., Kawata D., Cropper M., 2012b, *MNRAS*, 426, 167
- Jappsen A.-K., Klessen R. S., Larson R. B., Li Y., Mac Low M.-M., 2005, *A&A*, 435, 611
- Jog C. J., 1996, *MNRAS*, 278, 209
- Julian W. H., Toomre A., 1966, *ApJ*, 146, 810
- Koyama H., Inutsuka S.-I., 2000, *ApJ*, 1, 980
- Lin C. C., Shu F. H., 1964, *ApJ*, 140, 646
- Ma J., 2002, *A&A*, 395, 389
- Quillen A. C., Dougherty J., Bagley M. B., Minchev I., Comparetta J., 2011, *MNRAS*, 417, 762
- Roca-Fàbrega S., Valenzuela O., Figueras F., Romero-Gómez M., Velázquez H., Antoja T., Pichardo B., 2013, *MNRAS*, 432, 2878
- Sellwood J. A., Carlberg R. G., 2014, *ApJ*, 785, 137
- Shu F. H., Milione V., Roberts W. W., Jr, 1973, *ApJ*, 183, 819
- Springel V., Yoshida N., White S., 2001, *New Astron.*, 6, 79
- Vallée J. P., 2005, *AJ*, 130, 569
- Vázquez-Semadeni E., Gómez G. C., Jappsen A. K., Ballesteros-Paredes J., González R. F., Klessen R. S., 2007, *ApJ*, 657, 870
- Wada K., Koda J., 2004, *MNRAS*, 349, 270
- Wada K., Baba J., Saitoh T. R., 2011, *ApJ*, 735, 1

This paper has been typeset from a \LaTeX file prepared by the author.